IOP Publishing Physica Scripta
Phys. Scr. 95 (2020) 034006 (10pp) https://doi.org/10.1088/1402-4896/ab51ee

Water and hydrogen transport modelling through the membrane-electrode assembly of a PEM fuel cell

Viorel IONESCU

Department of Physics and Electronics, Ovidius University, Constanta, 900527, Romania

E-mail: v_ionescu@univ-ovidius.ro

Received 19 July 2019, revised 5 October 2019
Accepted for publication 28 October 2019
Published 6 February 2020

Abstract

Membrane electrode assembly (MEA) formed by a proton exchange membrane (PEM), two catalyst layers and two gas diffusion layers represent the heart of the PEM fuel cell system, being the place where the electrochemical reactions are developed in order to generate electrical power. Due to a complex water production and transportation process through the porous media of MEA, the water management represents one of the most critical issues for the low temperature PEM fuel cell systems, working at 30 °C–80 °C. In the present paper, a one-dimensional mass transport PEMFC model for evaluation of net water flux across the Nafion type membrane was implemented with the Comsol Multiphysis software, based on the finite element method. Hydrogen crossover phenomenon, which may cause a degradation of the reaction sites inside MEA, was also included in the model. The numerical model offered a reasonable prediction of the fuel cell electrical performance in the form of current–voltage characteristic after validation with experimental data from the literature. Fuel cell performance was investigated by modifying the temperature and pressure inside the cell, along with the relative humidity for reactant gases.

Keywords: water activity, ionomer phase, relative humidity, molar fraction, proton exchange membrane

(Some figures may appear in colour only in the online journal)

1. Introduction

The catalyst layer (CL), sometimes also called gas diffusion electrode (GDE) from membrane-electrode assembly (MEA) of a proton exchange membrane fuel cell (PEMFC) present an essential influence on the fuel cell performance, with fundamental impact on cell durability and cost. CL represents a microporous layer created by inter-mixing a microporous catalyst formed by platinum nanoparticles uniformly dispersed on a carbon black support (Pt/C) and a polymer phase for proton permeation (*ionomer*). Reactant gases and water will fill partially the pores of ionomer and Pt/C, giving rise to regions having three phases (solid, liquid and gas) very close to each other, named *three phase boundaries* [1]. Those three separate phases are gas pores for reactants, electron conducting electrode phase (carbon black) and ion conducting electrolyte phase (ionomer). Gas diffusion layers (GDLs), located outside the CL in the anodic and cathodic part of MEA are also porous and their primary role is related to electron conduction and reactant gas transport from bipolar plate channels. Pt particles can act as catalyst only if they are in contact with all the three phase boundaries [2].

Hydrogen crossover, phenomenon defined as the undesired diffusion of the gas from the anode to cathode through MEA represent one of the main problems related to the deterioration of Nafion-type membranes used in low temperature PEMFCs. Hydrogen crossover, which increase with temperature, pressure and humidity inside the cell can decrease open circuit voltage (OCV) and conduct to production of peroxide radicals at cathode, causing in this way the deterioration of Nafion membrane and CL inside MEA [3].

Near the boundary with ionomer phase, the current in the CL is carried mostly by ions and ionic conductivity is the most important here. Near the boundary containing gas diffusion medium, the most important are the gas permeability

and electronic conductivity of the medium [2]. So, the water management inside MEA will have a crucial importance for a proper fuel cell performance inside PEMFC systems working at temperatures of 60 °C–80 °C. The relative humidity inside MEA will be then critical in this way: humidity too high will produce mass transport limitations as a consequence of liquid water flooding of the gas pores at cathode (low electronic conductivity), whereas dry conditions will conduct to low ohmic conductivity in the ionomer. Each proton created at anode after hydrogen catalytic oxidation is transported to the cathode along with three molecules of water due to electro-osmotic drag phenomenon. H^+/H_2O transport at cathode is developed through the ionomer phase of CL and polymer electrolyte membrane.

Production of water at cathode after reaction of oxygen ions with protons and electrons will result in a gradient of the water concentration across the Nafion membrane and a consequent diffusion of water from the cathode to anode, as the *water back-diffusion* mechanism [4]. So, the net water flux across the membrane at any cell operating conditions represents a combination of diffusion and electro-osmotic drag.

Different mathematical models for water transport inside the MEA of PEMFC have been developed in the past, in order to predict power density losses of PEMFC due to activation, ohmic and mass transport over-potentials [5–7]. For this purpose, the net flux of water across membrane, which affects the ohmic over-potential, was estimated by considering the level of membrane hydration and the diffusion coefficient of water inside ionomer as a function of the membrane humidity content and the relationship of water activity in gas phase with water content in the membrane [4]. The combined effects of water transport through MEA, dependent on membrane hydration level and cathode water flooding was considered in one-dimensional model of PEMFC in order to estimate fuel cell electrical performance [8].

In this paper, it was developed a one-dimensional mass transport model for water through the MEA of PEMFC in order to investigate numerically the effect of backpressure from a real fuel cell testing system on the electrical performance at two different operating temperatures by evaluating different MEA parameters, like ionic conductivity, local current density and also the H_2 cross-over flux. The influence of relative humidity for reactant gases on the cell polarization curve was also investigated here.

2. Model formulation

In figure 1 is considered a MEA uni-dimensional model from a PEMFC cell based on seven layers, starting with interface I between Anode GDL and anode gas channel and finishing with interface VIII between cathode GDL and cathode gas channel. At the anode, a humidified H_2 flux is fed from the bipolar plate channel through GDL and MPL to the CL. A similar transport phenomenon is registered for humidified O_2 flux at cathode compartment. The three phase boundary will be developed at anode along interface III (gas–solid) and interface IV (solid–liquid) and at cathode along interfaces VI and V. Thickness for each of the domains inside the anode and cathode gas compartments (see the x axis values in figure 1) are considered starting from a 2D MEA numerical model [9].

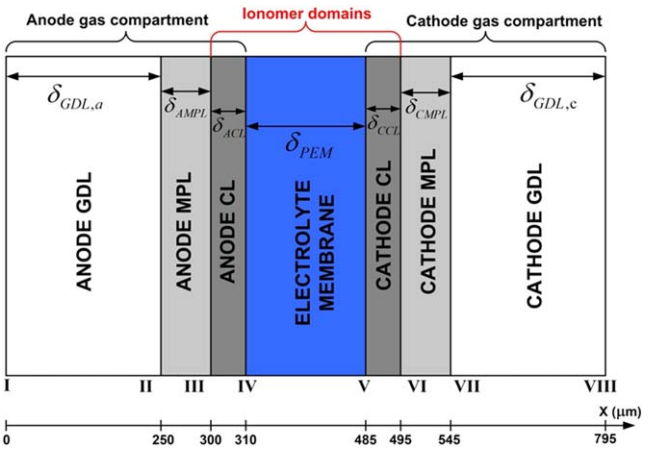

Figure 1. Schematic of the uni-dimensional MEA model domains in Comsol Mutiphysics.

2.1. Global variables for different domains

At the interfaces IV and V inside ionomer domains, both liquid and water vapor can dissolve in the electrolyte membrane by producing the absorption effect for dissolved water form, and in this way water will exist in three phases in the CLs: water, vapor and the dissolved phase [10].

Gas to ionomer phase transfer rate R_{H2O} (mol m^{-3} s^{-1}) at interfaces III and VI was expressed using reaction source/sink terms in the catalytic layers, starting from the finite-rate approach [11]:

$$R_{H_2O} = K_{H_2O}(a_{H_2O,gas} - a_{H_2O,ionomer}) \quad (1)$$

were the phase transfer rate constant K_{H2O} is assumed to be 10^6 mol m^{-3} s^{-1}.

The water gas phase activity in anode and cathode gas compartments was defined as [12]:

$$a_{H_2O,gas} = \frac{x_{H_2O,gas} \cdot P_i}{P_{vapor}}, \quad (2)$$

where $x_{H_2O,gas}$ is the numerically computed water molar fraction in the gas phase, P_{vapor} (Pa) is the water vapor pressure and $_{Pi}$ is the gas pressure at anode and cathode compartment (i = an,ca).

Water and hydrogen inlet molar fractions at anode compartment are calculated as:

$$x_{H_2O\_in,an} = \frac{RH_{an} \cdot P_{vapor}}{P_{an}}$$
$$x_{H_2\_in} = 1 - x_{H_2O\_in,an}. \quad (3)$$

Water, oxygen and nitrogen molar fractions at cathode compartment are considered as:

$$x_{H_2O\_in,ca} = \frac{RH_{ca} \cdot P_{vapor}}{P_{ca}}$$
$$x_{O_2\_in} = 0.21 \cdot (1 - x_{H_2O\_in,ca})$$
$$x_{N_2\_in} = 1 - x_{O_2\_in} - x_{H_2O\_in,ca}. \quad (4)$$

In relations (3) and (4), RH_{an} and RH_{ca} are the relative humidity at anode and cathode compartments, with values between 50% and 100% throughout simulations.

Water vapor pressure P_{vapor} (kPa) as a function of temperature was approximated with the Antoine equation in the temperature range $T = 50\,°C$–$100\,°C$ [13]:

$$\ln\left[\frac{P_{vapor}}{1Pa}\right] = 23.1963 - \frac{3816.44K}{T_{fc} - 46.13K} \quad (5)$$

with T_{fc} (K) as the PEM fuel cell operating temperature.

The water activity in the ionomer phase $a_{H_2O,ionomer}$ (dimensionless) along the ionomer domains was calculated as a function of water content λ using an empirical expression [14]:

$$\lambda = 0.043 + 17.71a_{H_2O,ionomer} - 39.85a^2_{H_2O,ionomer} + 36a^3_{H_2O,ionomer} \quad (6)$$

were λ can increase between 2 and 22 at 30 °C and as a consequence, protonic conductivity in the Nafion 117 membrane will increase linearly [14].

The concentration of H_2O dissolved in the ionomer (solved using the *Transport of Diluted Species* interface) was expressed as [15]:

$$C_{H_2O} = \frac{\rho\lambda}{EW}. \quad (7)$$

Concentration of protons H^+ in the ionomer was calculated as [15]:

$$C_{H^+} = \frac{C_{H_2O}}{\lambda}. \quad (8)$$

In the equation (7), $EW = 1100\,g\,mol^{-1}$ represent the equivalent weight of the ionomer [15] and ρ is the humidity-dependent density of the ionomer, given by [15]:

$$\rho = \frac{1.98 + 0.00\,324\lambda}{1 + 0.0648\lambda}. \quad (9)$$

Water diffusion coefficient in ionomer D_{H2O} ($m^2\,s^{-1}$) is also dependent on λ, considered here in the form an interpolation polynomial function derived from experimental data [4]:

$$D_{H2O} = 6.31 \times 10^{-7}(\lambda - 0.0209\lambda^2 - 0.501). \quad (10)$$

It was shown experimentally that ionic conductivity of Nafion membrane depends on the water content and operating temperature. Zawodzinski *et al* [14] measured the temperature dependence of the conductivity on a Nafion 117 membrane immersed in liquid water in the temperature range from 25 to 90 °C and also proton conductivity as a function of water content λ, reporting that λ was constant at 22 over this range of temperature. Based on these measurements, Springer *et al* [6] correlated the proton conductivity using the following expression:

$$\sigma_l = (0.005\,139\lambda - 0.00\,326) \times \exp\left[1268\left(\frac{1}{303K} - \frac{1}{T_{fc}}\right)\right](S\,cm^{-1}) \quad (11)$$

Hydrogen cross-over flux along the membrane Φ_{H2} ($mol\,cm^{-2}\,s^{-1}$) was defined as the concentration difference of the H_2 molecules over the Nafion 117 membrane thickness $L_m = 175\,\mu m$ under the form of Fick's law [16]:

$$\phi_{H_2} = D_{H_2,ionomer} \cdot \frac{\Delta C_{CL,a}}{L_m}, \quad (12)$$

where $\Delta C_{CL,a}$ is the computationally calculated variation of H_2 concentration at anode CL and $D_{H_2,ionomer}$ is the hydrogen diffusion coefficient in the ionomer ($cm^2\,s^{-1}$).

D M Bernardi and M W Verbrugge [17] reported two different diffusivities of dissolved hydrogen in Nafion 117 membrane for PEMFC tested at operating temperatures of 80 °C and 95 °C: $2.59 \cdot 10^{-6}$ and $3.48 \cdot 10^{-6}\,cm^2\,s^{-1}$, considered also during simulations in expression (12).

2.2. Governing equations in comsol multiphysics interfaces

Electric charge conservation is based on two currents: an ionic current formed by protons passing through electrolyte membrane from anode to cathode (i_l) and an electronic current formed by electrons travelling the solid matrix of GDL and CL (i_s). The general continuity equations from *Secondary Current Distribution* interface are derived from Ohm's law in the form of:

$$\nabla i_l = Q_l, \text{ with } i_l = -\sigma_l \nabla\phi_l, \quad (13)$$
$$\nabla i_s = Q_s, \text{ with } i_s = -\sigma_s \nabla\phi_s, \quad (14)$$

where σ_l is the electrolyte conductivity, calculated with expression (11) and Q_l, Q_s ($A\,m^{-3}$) denotes general current source terms (considered zero here).

The solid phase conductivity σ_s is associated with σ_{GDL} for $\delta_{GDL,a}$ and $\delta_{GDL,c}$ domains, with σ_{MPL} for δ_{AMPL} and δ_{CMPL} domains and with σ_{CL} for δ_{ACL} and δ_{CCL} domains. During the simulations, $\sigma_{GDL} = 10.000\,S\,m^{-1}$, $\sigma_{CL} = 1000\,S\,m^{-1}$ and $\sigma_{MPL} = 100\,S\,m^{-1}$ [18].

The electric potentials associated with liquid and solid phase are denoted here as ϕ_l and ϕ_s, respectively. In the anode gas compartment, $\phi_l = \phi_s = 0$ and in the cathode compartment, $\phi_l = 0$, $\phi_s = E_{cell} = 0.9\,V$.

For δ_{ACL} and δ_{CCL} domains are available also the following equations [19]:

$$\nabla i_l = Q_l + i_{v,total};\ i_l = -\sigma_{l,eff}\nabla\phi_l, \quad (15)$$

$$\sigma_{l,\text{eff}} = \varepsilon_l^{1.5} \cdot \sigma_l, \tag{16}$$

$$\nabla i_s = Q_s - i_{v,\text{total}};\ i_l = -\sigma_s \nabla \phi_s, \tag{17}$$

$$i_{v,\text{total}} = \sum_m i_{v,m}, \tag{18}$$

$$i_{v,m} = a_v \cdot i_{\text{loc},m} \tag{19}$$

were expression (16) represents the correction for Bruggeman effective conductivity [20], with ε_l as electrolyte volume fraction of CL and $i_{v,\text{total}}$ is the total volumetric current density (A m^{-3}), which include the contributions from electrochemical reactions developed at anode and cathode CL.

In relation (19), m indicates the anodic a and cathodic c components of the current $i_{v,\text{total}}$ and a_v (1/m) represents the active surface area of CL. In order to evaluate a_v, the actual platinum surface area based on the Pt loading and Pt particle size is first calculated.

An effective Pt surface ratio ε_l is considered for the expression of the surface area actually utilized inside the oxygen reduction reaction [21]:

$$a_v = \varepsilon_l a_{\text{Pt}}, \tag{20}$$

where a_{Pt} is the specific platinum surface area per unit CL volume (m^2 m^{-3}), which is equal to the platinum loading divided by the CL thickness t_{cl} multiplied by the specific surface area of the platinum particles, S_{ac} in the form of expressions [21]:

$$a_{\text{Pt}} = \left(\frac{m_{\text{Pt}}}{t_{\text{cl}}}\right) \cdot S_{\text{ac}}, \tag{21}$$

$$S_{\text{ac}} = \frac{3}{r_{\text{Pt}} \cdot \rho_{\text{Pt}}}. \tag{22}$$

In relation (22), r_{Pt} represents the radius of an individual Pt particle and $\rho_{\text{Pt}} = 21.45$ g cm^{-3} is the Pt density. A CL with thickness $t_{\text{cl}} = 15$ μm and $\varepsilon_l = 0.75$, having a Pt loading $m_{\text{Pt}} = 0.4$ mg cm^{-2} was characterized by $r_{\text{Pt}} = 2.5$ nm [19]. MEA assembly used inside a PEMFC cell, experimentally tested at different backpressures was based on a Nafion 117 membrane and a CL with Pt loading of 1 mg cm^{-2} at anode and cathode [22].

So, in the present simulations based on experimental tests [22], we selected an individual Pt particle radius $r_{\text{Pt}} = 6$ nm for the same catalyst parameters $t_{\text{cl}} = 15$ μm and $\varepsilon_l = 0.75$. By using the expressions (20)–(22) it was obtained $a_v = 1.16 \cdot 10^7$ (1/m).

The local exchange current density i_{loc} (A m^{-2}) was predefined inside the interface using the simplified Butler–Volmer equations [21, 23] for δ_{ACL} domain:

$$i_{\text{loc},a} = i_{0,\text{H}_2}\left[C_R \exp\left(\frac{\alpha_a F}{\text{RT}}\eta_{\text{act},a}\right) - C_0 \exp\left(-\frac{\alpha_c F}{\text{RT}}\eta_{\text{act},a}\right)\right] \tag{23}$$

with i_{0,H_2}(A m^{-2}) as the exchange current density at anode, the anodic and cathodic transfer coefficients: $\alpha_a = 0.5$ and $\alpha_c = 1.5$ were considered for electrochemical reactions at anode CL, C_R is the reduced species expression at anode in terms of molar fraction (numerically evaluated through simulations) and $C_0 = 1$ is the oxidized species expression, also expressed as molar fraction.

For δ_{ACL} domain it was defined a similar Butler–Volmer type equation:

$$i_{\text{loc},c} = i_{0,O_2}\left[C_R \exp\left(\frac{\alpha_a F}{\text{RT}}\eta_{\text{act},c}\right) - C_0 \exp\left(-\frac{\alpha_c F}{\text{RT}}\eta_{\text{act},c}\right)\right] \tag{24}$$

with i_{0,O_2}(A m^{-2}) as the exchange current density at cathode, $\alpha_a = 3.5$ and $\alpha_c = 0.5$, $C_R = a^2_{\text{H}_2\text{O,ionomer}}$ and C_0 is numerically computed during simulations.

Ubong *et al* [23] reported in their 3D modeling study for a PEMFC unit cell using Comsol Multiphysics software the following values for the kinetic parameters involved in Butler–Volmer equations: $a_{\text{Pt},a} \cdot i_{0,\text{H}_2} = 1 \times 10^9$ A m^{-3} and $a_{\text{Pt},c} \cdot i_{0,\text{O}_2} = 3 \times 10^3$ A m^{-3}. Using the equation (21), it was established here that $a_{\text{Pt},a} = a_{\text{Pt},c} = 1.55 \cdot 10^7$ (1/m), and the corresponding exchange current densities were $i_{0,\text{H}_2} = 64.5$ A m^{-2} and $i_{0,\text{O}_2} = 1.9 \cdot 10^{-4}$ A m^{-2}. Those two values were also used during numerical simulations, for calculation of the currents $i_{\text{loc},a}$ and $i_{\text{loc},c}$.

The electrochemical activation potential η_{act} between CL solid matrix and PEM electrolyte at anode and cathode (at boundaries IV and V) was defined as [24]:

$$\eta_{\text{act},a} = \phi_s - \phi_l - E_{\text{eq},\text{H}_2}$$
$$\eta_{\text{act},c} = \phi_s - \phi_l - E_{\text{eq},\text{O}_2}, \tag{25}$$

where the potential loss for the hydrogen oxidation was neglected ($E_{\text{eq},}\text{H}_2 = 0$) [23] and thermodynamic equilibrium potential for oxygen reduction was derived from Nernst equation [25, 26]:

$$E_{\text{eq},O_2} = E_0 - 0.85 \times 10^{-3}(T_{fc} - 298.15) + 4.3085 \times 10^{-5} T_{fc} \cdot [\ln(p_{\text{H}_2\text{an}}) + \ln(p_{\text{O}_2\text{ca}})/2]. \tag{26}$$

In relation (26), p_{H2an} and p_{O2ca} are the partial pressures for hydrogen and oxygen inside the PEM fuel cell system. In order to validate the present numerical model, we considered the values $p_{\text{H2an}} = 1.93$ atm and $p_{\text{O2ca}} = 0.085$ atm, evaluated through experimental measurements of a PEMFC single cell system [22]. The theoretical initial open circuit voltage is $E_0 = 1.18$ V, considering water production in vapor phase at cathode [27].

Using Fick's laws, *Transport of diluted species* interface can offer the solution of the diffusion problem for water transport trough ionomer domains (δ_{PEM}, δ_{ACL} and δ_{CCL}), under the form of equation [28]:

$$\nabla \cdot J_i = R_i$$
$$J_i = -D_i \nabla c_i - z_i u_{m,i} F c_i \nabla V. \tag{27}$$

Table 1. Operating backpressures and anodic/cathodic pressures inside the fuel cell system considered for simulation in the numerical PEMFC model.

Backpressure		Cell operating temperature							
		80 °C				95 °C			
$P_{b,a}$(kPa)	$P_{b,c}$(kPa)	P_{an}(atm)	P_{ca}(atm)	p_{H2an}(atm)	p_{O2ca}(atm)	P_{an}(atm)	P_{ca}(atm)	p_{H2an}(atm)	p_{O2ca}(atm)
0	0	2.21	0.73	1.74	0.055	2.39	0.91	1.55	0.016
50	50	2.45	0.97	1.98	0.106	2.64	1.16	1.80	0.067
70	70	2.55	1.07	2.08	0.127	2.74	1.26	1.90	0.088
90	90	2.65	1.17	2.18	0.148	2.83	1.35	2	0.109

In the above relations, i indices is associated with H_2O species; J_i represent a flux term (mol m^{-2} s^{-1}), with D_i (m^2 s^{-1}) as the water diffusion coefficient in ionomer, $c_i = C_{H2O}$ (see relation (5)), $z_i = 1$ is the H_2O charge number, F is the Faraday constant (C mol^{-1}), V is the electric potential (V).

The water mobility in ionomer $u_{m,i}$ (mol s Kg^{-1}) is evaluated using the relation:

$$u_{m,i} = \frac{n_d \cdot \sigma_l \cdot F^2}{C_{H_2O}} \tag{28}$$

were the net electro-osmotic drag coefficient (H_2O/H^+) n_d considered here was measured at values of 0.3–0.35 in a PEMFC system with Nafion 117 membrane at a current density of 0.5 A m^{-2} and operating parameters like a cathode air pressure of 1 atm, operating temperature of 80 °C and RH (%) between 50 and 100 at cathode [29].

The species reaction rate R_i (mol m^{-3} s^{-1}) is pre-defined on δ_{CCL} domain under the form of:

$$R_i = \frac{\nu_{c,H_2O\_inomer} \cdot i_v}{n \cdot F}, \tag{29}$$

where number of participant electrons $n = 4$ and stoichiometric coefficient for water in ionomer phase $\nu_{c,H_2O\_inomer} = 2$.

Transport of Concentrated Species interface was used for modeling chemical species transport: hydrogen and air mixture at anode and cathode, respectively, by solving for the mass fractions of the species. Conservation of species was solved for anode and cathode gas compartments using the Maxwell–Stefan diffusion model, starting from the general expression [30]:

$$\nabla \cdot j_i + \rho(u \cdot \nabla)\omega_i = R_i \tag{30}$$

were ρ is the overall mass density of the hydrogen or air mixture, u is the fluid velocity (m s^{-1}), ω_i is the mass fraction of the species i at anode (H_2, H_2O) or cathode (O_2, N_2, H_2O).

In formulation (30), R_i is related with mass transfer to ionomer phase, and it was specified $R_{H2} = R_{O2} = R_{N2} = 0$. Diffusion rate of water vapor in ionomer phase at anode and cathode was considered as: $R_{w,H2O,an} = R_{w,H2O,ca} = -R_{H2O} \cdot M_{H2O}$ (Kg m^{-3} s^{-1}), with M_{H2O} (g/mol) as water molecular mass.

The relative diffusion flux vector j_i is pre-defined here as:

$$j_i = -\rho\omega_i \sum_{k=1}^{N} \tilde{D}_{ik} d_k - \frac{D_i^T}{T}\nabla T, \tag{31}$$

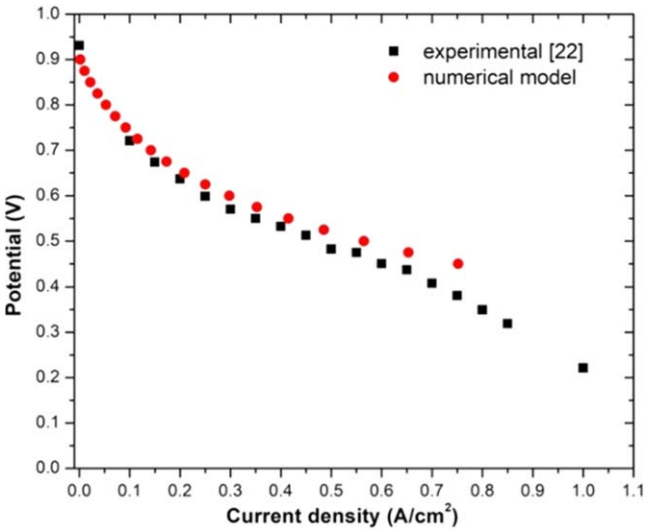

Figure 2. Comparative illustration of the polarization curves for the experimental test and numerical PEMFC model.

where $\tilde{D}_{ik}$ (m^2 s^{-1}) are the multicomponent Fick diffusivities and D_i^T is the thermal diffusion coefficient (kg m s^{-1}), neglected in this simulation. The diffusional driving force d_k (1 /m) is pre-defined inside the interface as:

$$d_k = \nabla x_k + 1/p \cdot [(x_k - \omega_k)\nabla p] \tag{32}$$

were x_k is the mole fraction of k species at anode and cathode, pressure p being replaced during simulations by the experimental average pressure P_{an} and P_{ca} from table 1.

The binary diffusivities $\tilde{D}_{ik}$ from expression (31) have been calculated starting from empirical correlations [23].

3. Results and discussions

In order to validate the numerical model, an experimental polarization curve for a PEMFC cell was considered from a previous study, presented in detail elsewhere [22].

One set of experiments was performed on a single PEM fuel cell unit using a BEKKTECH BT-552 PEMFC test station, at a cell temperature of 80 °C, 80% relative humidity of reactant gases and anode and cathode inlet pressures of 400 kPa and 100 kPa, respectively, with cathodic/anodic backpressures $P_{b,c}/P_{b,a}$ of 20/30 kPa and the average

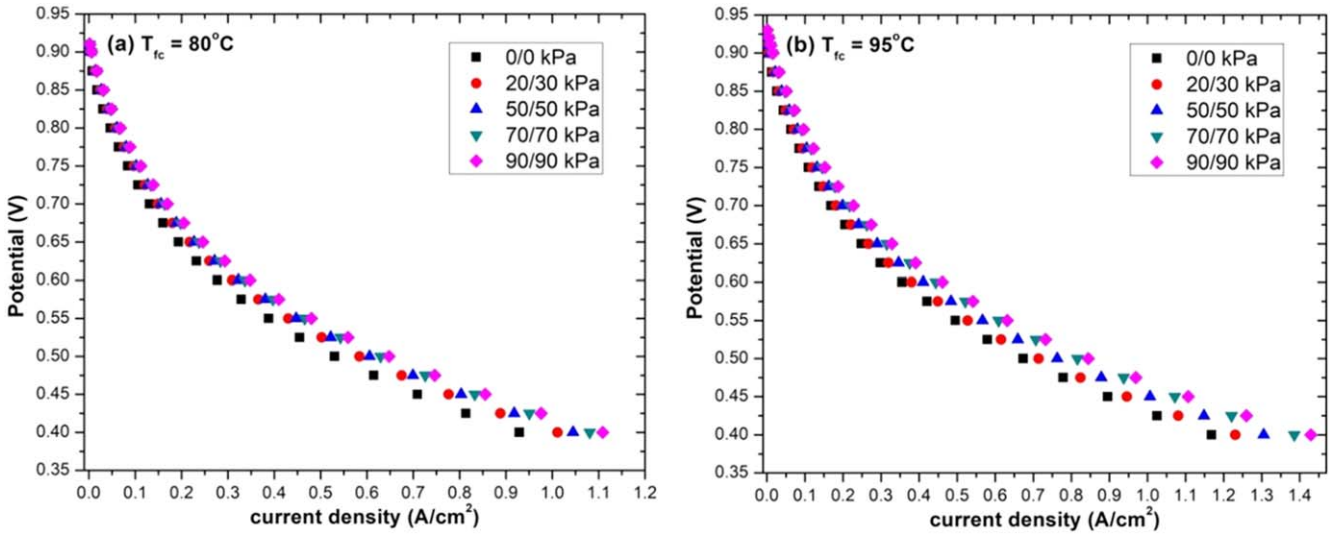

Figure 3. Simulated polarization curves for the PEMFC model at different values of $P_{b,a}/P_{b,c}$ (kPa), registered for two cell temperatures.

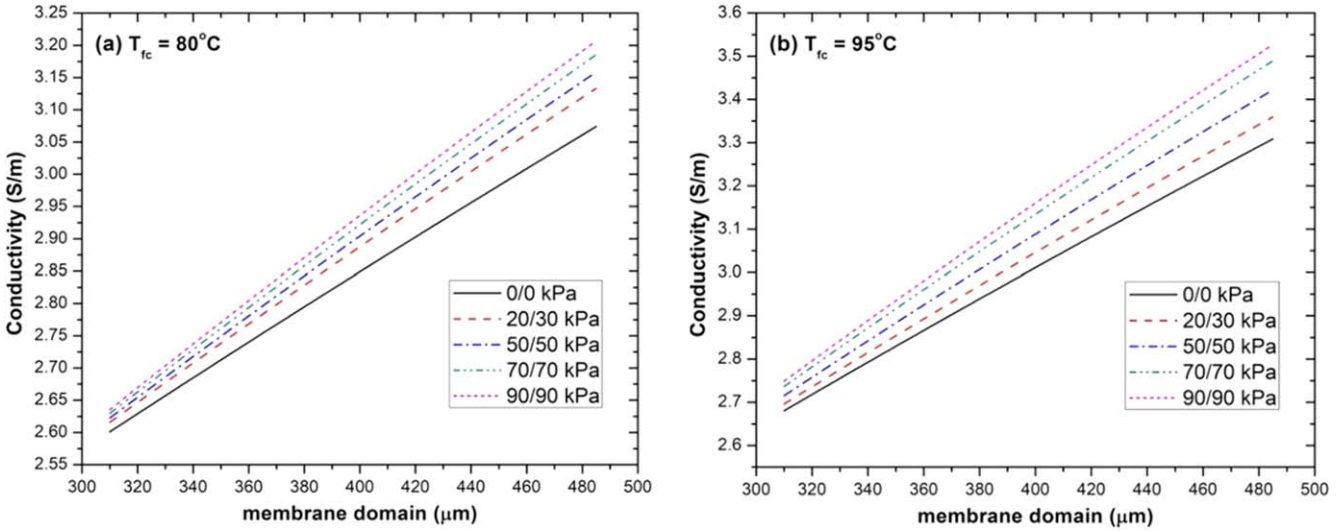

Figure 4. Variations of ionic conductivity across the Nafion electrolyte membrane domain at different values of $P_{b,a}/P_{b,c}$ (kPa), registered at $E_{cell} = 0.6$ V for two cell temperatures.

pressures of humidified gases crossing the fuel cell at anode and cathode: $P_{an} = 2.31$ atm, $P_{ca} = 0.87$ atm [22].

As it can be seen from figure 2, a good matching between the experimental and numerical curves was attained in the activation loss region for the voltage (till about 0.1 A cm^{-2}). A reasonable difference between the two set of values was observed in the ohmic loss region (0.1–0.7 A cm^{-2}), were only the resistance due to the transport of protons through the electrolyte membrane was considered as a voltage loss inside this simplified model. The voltage loss due to the limitation of oxygen transport at the reaction sites, observed experimentally starting with 0.7 A cm^{-2} was neglected in the model.

Another set of measurements was conducted with the same BEKKTECH BT-552 testing system under similar humidity and temperature testing conditions, but at different inlet pressures for anode and cathode: 300 kPa and 200 kPa, respectively and at two different backpressures $P_{b,c}/P_{b,a}$ (kPa) : 30/30 and 70/70 [31, 32]. From those measurements it was observed an important increase of exergetic efficiency, with 1.5%–11% between current densities of 0.1–0.7 A cm^{-2}, for one of the fuel cells tested at the higher backpressure ($P_{b,c}/P_{b,a} = 70/70$ kPa) [31]. This exergy gain was attained with the compromise of higher voltage oscillations at current densities over 0.4 A cm^{-2} and with lower voltage stability at a constant load of 0.5 A cm^{-2} [32]. It was also demonstrated experimentally by other researchers that a backpressure increasing from 1 to 3 atm inside a PEM fuel cell testing system at cell temperature of 70 °C and 100% relative humidity produced an enhancement of the average oxygen partial pressure inside the cell and also an increase in the fuel cell electrical performance [33]. Generally, an increase of the fuel cell temperature will improve its electrical performance,

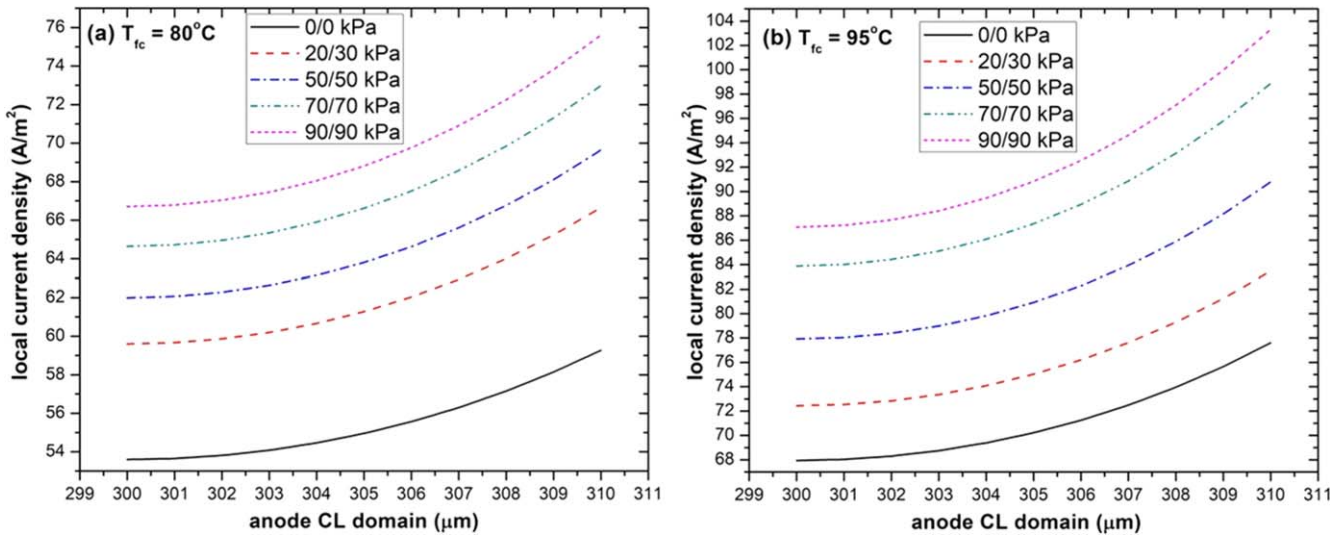

Figure 5. Local current density distribution across the anode CL domain at different values of $P_{b,a}/P_{b,c}$ (kPa), registered at $E_{cell} = 0.6$ V for two different T_{fc}.

but higher operating temperatures can lead to membrane dehydration, increased hydrogen crossover rate, and the degradation of components such as electrocatalysts, gasket materials, and bipolar plates [34].

So, starting from all those experimental observations regarding the fuel cell behavior at different backpressures and operating temperatures, we proposed to investigate numerically in the first part of this study the level of improvement for the fuel cell electrical performance under superior backpressure and operating temperature values. The main target was to establish the opportunity of possible future tests of the fuel cell at these higher operating parameters in the conditions of the negative effects specified above. In order to study the influence of backpressure inside a PEMFC testing system on the fuel cell performance at two different cell temperatures using the present one-dimensional model, another set of values have been considered for $P_{b,a}/P_{b,c}$ at anodic/cathodic inlet pressures of 400 kPa and 100 kPa, with the corresponding calculated values for p_{H2an} and p_{O2ca}, respectively for P_{an} and P_{ca} (see table 1). The mathematical formulation used for obtaining those average pressures inside the cell is presented elsewhere [22].

The simulated polarization curves for the PEMFC model at cell temperatures of 80 °C and 95 °C are presented in figure 3, at different anodic/cathodic backpressures $P_{b,a}/P_{b,c}$(kPa). We could observe here a clear electrical performance enhancement in the fuel cell model after the increasing of $P_{b,a}/P_{b,c}$ from 0/0 kPa to 90/90 kPa, current density at 0.6 V (in the middle of ohmic loss region) being increased with over 20% at 80 °C and with 30% at 95 °C. As a consequence of backpressure increasing in a PEMFC system, the partial pressure of the reaction gases (O_2 and H_2) within the combustion cell will increase (see $p_{H2,an}$ and $p_{O2,ca}$ in table 1), the diffusion of reactant gases at the active catalyst sites will be enhanced and the exchange current density will increase.

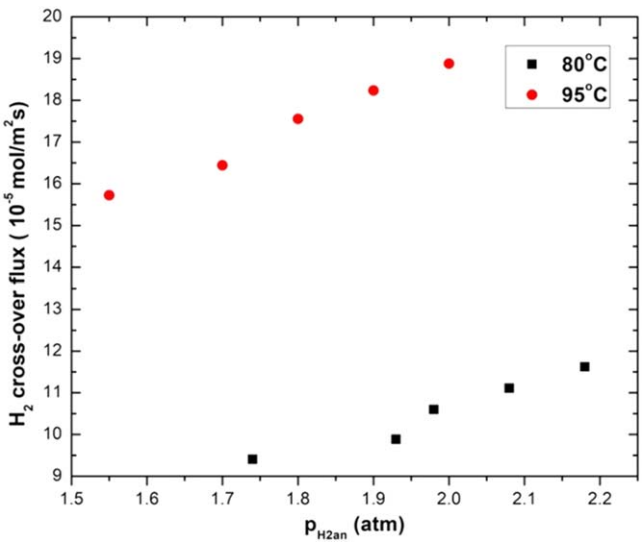

Figure 6. Variation of the hydrogen cross-over flux along the electrolyte membrane at different H_2 partial pressures.

From figures 3(a) and (b) we observed also an enhancement in the fuel cell electrical performance after modifying T_{fc} from 80 °C to 95 °C, current density at 0.6 V increasing in this way from 0.348 to 0.461 A cm^{-2} for the model simulated at $P_{b,a}/P_{b,c} = 90/90$ kPa. This phenomenon can be explained by the increase in the gas diffusivity and membrane conductivity at higher temperature and also by the reduction of activation losses due to the increase of exchange current density, as it can be seen from the variations of ionic conductivity along the membrane domain, respectively of the local current density along the CL anode domain presented in figure 4 and in figure 5. We observed here that the smallest parameter improvement from one set of backpressures $P_{b,a}/P_{b,c}$ to another was registered between 70/70 and 90/90 kPa, were was observed also the smallest electrical performance improvement of the cell (see figure 3).

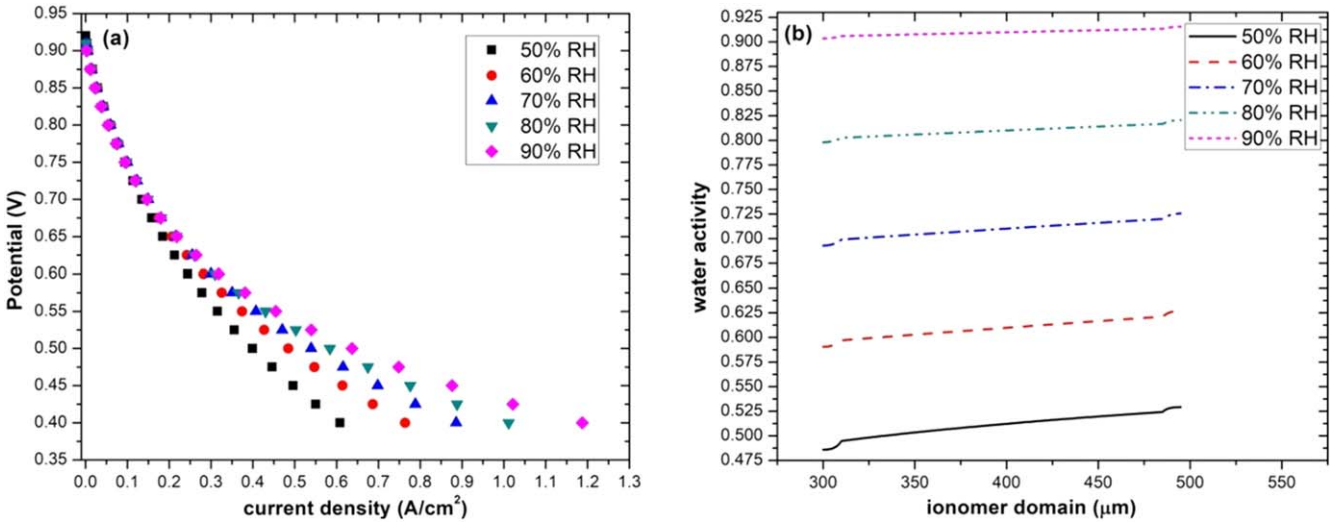

Figure 7. Influence of relative humidity RH (%) on: (a) the polarization curve and (b) ionomer water activity for the PEMFC model at $E_{\text{cell}} = 0.6$ V.

The performance drop of PEMFC, registered at lower temperatures was associated with a limited proton transfer process to the catalyst sites, developed mainly in the ionomer regions of the MEA [35].

As we can observe in figures 4(a) and 5(a) in the case of simulations performed at $T_{fc} = 80\,^{\circ}\text{C}$, an evident difference was registered between the protonic conductivities of the membrane and between local current densities at CL anode simulated at anodic/cathodic backpressures of 20/30 kPa and without backpressure (0/0 kPa). At the interface between electrolyte membrane and cathode CL domains (at 485 μm) it was registered conductivities of 3.13 S m^{-1} and 3.07 S m^{-1} for the first two set of backpressures (see figure 4(a)), and at the interface between anode CL and membrane domain (at 310 μm), local current density increased from 59.26 A m^{-2} to 66.64 A m^{-2} between the same anodic/cathodic backpressures (see figure 5(a)).

This improvement of the conductivity an local current density is reflected in a clear reduction of ohmic losses for the equivalent current density plot generated at 20/30 kPa, by comparing with the plot generated at 0/0 kPa inside the PEMFC model (see figure 3(a)).

Tests performed on a single cell PEMFC station at 80 °C indicated an improved MEA conductivity and preservation of OCV after 100 h of operation at a backpressure of 69 kPa, by comparing with the results of the experiment conducted without backpressure [36].

It was reported from experimental tests developed at 80 °C and 50% RH for a PEMFC system with Nafion 117 membrane a gradual increase of the H_2 crossover flux rate as a consequence of backpressure increasing [37], due to the fact that an increased partial pressure of hydrogen will determine a pressure drop enhancement inside the cell. So, the H_2 crossover rate should increase along with H_2 partial pressure enhancement, process demonstrated experimentally by Schalenbach *et al* [16].

So, knowing that a high operating backpressure can involve a series of negative effects like a H_2 crossover, in figure 6 are presented the variations of hydrogen cross-over flux Φ_{H2} at different average partial pressures of hydrogen, calculated at different backpressures $P_{b,a}/P_{b,c}$ (see table 1) for both operating temperatures, with numerical model simulated at $E_{\text{cell}} = 0.6$ V and 80% RH. A linear increase of the Φ_{H2} along with p_{H2an} increasing was seen in figure 6 for both T_{cell} under study. For example, at 80 °C, Φ_{H2} increased from $9.4 \cdot 10^{-5}$ mol m^{-2} s^{-1} till $11.62 \cdot 10^{-5}$ mol m^{-2} s^{-1} after modifying backpressure from 0/0 to 90/90 kPa.

Cheng *et al* [37] measured and observed an increase of H_2 crossover rate through Nafion 117 based MEAs with over 25% (at 70% RH and $P_{b,a} = 101$ kPa) after increasing cell temperature from 80 °C to 100 °C, and suggested that H_2 crossover rate enhancement is due the increasing of H_2 permeability coefficient, directly related to the H_2 solubility and diffusion coefficients. It was demonstrated that an increase in temperature can effectively increase the H_2 permeability coefficient at any given backpressure and RH and, similarly, increasing backpressure can always increase the value of the H_2 permeability coefficient at any given RH [37]. The hydrogen permeation flux density through a fully hydrated Nafion 117 membrane tested at 80 °C had a reported a value of $5 \cdot 10^{-5}$ mol m^{-2} s^{-1} at a H_2 partial pressure of 1.98 atm [16].

In the final part of this numerical study it was simulated the impact of the relative humidity RH on the fuel cell model performance. A proper humidification is necessary in order to reduce resistive losses in a cell and to maintain a low ionic resistance throughout the membrane by increasing its conductivity [38].

In figure 7 was presented the simulated current–voltage characteristics for the experimentally validated model at $T_{fc} = 80\,^{\circ}\text{C}$ and $P_{b,a}/P_{b,c} = 20/30$ kPa with RH(%) modified between 50 and 90, along with corresponding variation for

ionomer water activity $a_{H_2O,ionomer}$ across the ionomer domain.

We could see from figure 7 a major dropping of current density in the ohmic loss region of the polarization curves, from 0.094 to 0.058 A cm^{-2} at 0.8 V and from 0.637 to 0.399 A cm^{-2} at 0.5 V when RH was reduced from 90% to 50%. This behavior is correlated directly with the reduction of water activity in the ionomer domains, from about 0.9 till about 0.5, as we could observe in figure 7(b), which will reduce the ionic conductivity of the Nafion membrane and will lead to smaller values of current densities than better hydrated cases. The main reason for the reduction of the water activity within the catalyst and gas diffusion layers is the fact the water produced due to the electrochemical reaction is partially dragged from the anode CL to the membrane in order to compensate the dehydrated condition caused by the decrease in the relative humidity at the flow channel inlet [39].

Zhang *et al* [40] studied the effect of relative humidity on Nafion-based MEA PEM fuel cell system at 120 °C and a backpressure of 1 atm by decreasing RH from 100% to 25%, and observed that the cell electrical performance was significantly depressed due to reduction of various parameters, like protonic conductivity of the membrane, reactant mass diffusion and electrode reaction rates, pressure drops across the flow fields.

4. Conclusions

A uni-dimensional numerical model for a PEM fuel cell was successfully implemented in this study, after experimental validation of the polarization curve in the activation and ohmic loss regions.

Numerical simulation performed at $T_{fc} = 80$ °C and at cell potential of 0.6 V, with backpressure increasing from 0 to 90 kPa revealed an enhancement of current density with over 20% as a consequence of a maximum ionic conductivity increasing of 4% in the Nafion membrane, local current density at anode CL increasing with about 20%.

After increasing T_{fc} from 80 °C to 90 °C at a backpressure of 90 kPa, PEMFC numerical model indicated an enhancement of the current density with 24% at a potential of 0.6 V.

An important ohmic loss enhancement of about 38% was observed in the current–voltage characteristic of the PEMFC model when RH was reduced from 90% to 50%, with a decreasing of over 40% for the water activity in the ionomer domains.

References

[1] Chapparo M A, Folgado M A, Fereira–Aparicio P, Martin A J and Daza L 2010 Microstructure of electrospray deposited catalyst layers for PEMFC electrodes *ECS Trans.* **26** 197–205

[2] Grot W 2011 *Fluorinated Ionomers* 2nd (Oxford: Elsevier Inc) p 159

[3] Francia C, Ijeri V S, Specchia S and Spinelli P 2011 Estimation of hydrogen crossover through nafion membranes in PEMFCs *J. Power Sources* **196** 1833–9

[4] Motupally S, Becker A J and Weidner J W 2000 Diffusion of water in nafion 115 membranes *J. Electrochem. Soc.* **147** 3171–7

[5] Yi J S and Nguyen T V 1998 An along-the-channel model for proton Exchange membrane Fuel cells *J. Electrochem. Soc.* **145** 1149–59

[6] Springer T E, Zawodzinski T A and Gottesfeld S 1991 Polymer electrolyte fuel cell model *J. Electrochem. Soc.* **138** 2334–42

[7] Nguyen T V and White R E 1993 A water and heat management model for proton-exchange-membrane fuel cells *J. Electrochem. Soc.* **140** 2178–86

[8] Li Y and Lv H 2018 The combined effects of water transport on proton exchange membrane fuel cell performance *Chem. Eng. Trans.* **65** 691–6

[9] Dobson P 2011 Investigation of the polymer electrolyte membrane fuel cell catalyst layer microstructure *MSc Thesis* University of Alberta, Canada https://doi.org/10.7939/R3VD0R

[10] Xu C, Zhao T S and Yang W W 2008 Modeling of water transport through the membrane electrode assembly for direct methanol fuel cells *J. Power Sources* **178** 291–308

[11] Yang W W and Zhao T S 2007 Two-phase, mass-transport model for direct methanol fuel cells with effect of non-equilibrium evaporation and condensation *J. Power Sources* **174** 136

[12] Motupally S, Becker A J and Weidner J W 2000 Diffusion of water in nafion 115 membranes *J. Electrochem. Soc.* **147** 3171–7

[13] Vetter R and Schumacher J O 2019 Free open reference implementation of a two-phase PEM fuel cell model *Comput. Phys. Commun.* **234** 223–34

[14] Zawodzinski T Z *et al* 1993 Water uptake by and transport through Nafion 117 membranes *J. Electrochem. Soc.* **140** 1041–7

[15] Sethuraman V A, Weidner J W, Haug A T, Motupally S and Lesia V 2008 Protsailo, hydrogen peroxide formation rates in a PEMFC anode and cathode *J. Electrochem. Soc.* **155** B50–7

[16] Schalenbach M, Hoefner T, Paciok P, Carmo M, Lueke W and Stolten D 2015 Gas permeation through nafion. part 1: measurements *J. Phys. Chem.* C **119** 25145–55

[17] Bernardi D M and Verbrugge M W 1992 A mathematical model of the solid-polymer-electrolyte fuel cell *J. Electrochem. Soc.* **139** 2477–91

[18] Nanadegani F S, Lay E N and Sunden B 2019 Effects of an MPL on water and thermal managementin a PEMFC *Int. J. Energy Res.* **43** 274–96

[19] Xing L, Das P K, Song X, Mamlouk M and Scott K 2015 Numerical analysis of the optimum membrane/ionomer water content of PEMFCs: The interaction of nafion ionomer content and cathode relative humidity *Appl. Energy* **138** 242–57

[20] Das P K, Li X and Liu Z S 2010 Effective transport coefficients in PEM fuel-cell catalyst and gas diffusion layers: beyond Bruggeman approximation *Appl. Energy* **87** 2785–96.

[21] Sun W, Peppley B A and Karan K 2005 An improved two-dimensional agglomerate cathode model to study the influence of catalyst layer structural parameters *Electrochim. Acta* **50** 3359–74

[22] Andronie A, Stamatin I, Girleanu V, Ionescu V and Buzbuchi N 2019 Simplified mathematical model for polarization curve validation and experimental performance evaluation of a PEM fuel cell system *Proc. Manuf.* **32** 810–19

[23] Ubong E U, Shi Z and Wang X 2009 Three-dimensional modeling and experimental study of a high temperature PBI-based PEM fuel cell *J. Electrochem. Soc.* **156** 1276–82

[24] Kulikovsky A A 2015 Potentials near a curved anode edge in a PEM fuel cell: analytical solution for placing a reference electrode *J. Electrochem. Soc.* **162** F1191–8
[25] Rojas A C, Lopez G L, Gomez-Aguilar J F, Alvarado V M and Luz Sandoval Torres C 2017 Control of the Air Supply Subsystem in a PEMFC with Balance of Plant Simulation *Sustainability* **9** 1–23
[26] Feroldi D and Basualdo M S 2012 *PEM Fuel Cells with Bio-Ethanol Processor Systems, 49 Green Energy and Technology* (London: Springer) p 66
[27] Breeze P 2019 *Power Generation Technologies* 3rd edn (UK: Newnes Elsevier) p 155
[28] Banerjee T, Ghoshal S and Bhattacharya B B 2017 COMSOL-based design and validation of dilution algorithm with continuous-flow lab-on-chip *INAE Lett* **2** 55–63
[29] Yan Q, Toghiani H and Wu J 2006 Investigation of water transport through membrane in a PEM fuel cell by water balance experiments *J. Power Sources* **158** 316–25
[30] Bothe D 2011 On the maxwell-stefan approach to multicomponent diffusion *Parabolic Problems. Progress in Nonlinear Differential Equations and Their Applications* ed J Escher *et al* (Basel: Springer) pp 81–93
[31] Ionescu V, Buzbuchi N, Andronie A, Stamatin I and Girleanu V 2019 Exergy analysis of a PEM fuel cell system with different bipolar plate flow fields, 2019 *11th Int. Symp. on Advanced Topics in Electrical Engineering (ATEE) (Bucharest, Romania)* p 1–6
[32] Ionescu V, Buzbuchi N, Andronie A, Stamatin I and Girleanu V 2019 Current - voltage variation and voltage stability at constant load for a PEMFC system with different bipolar plate flow fields, 2019 *11th Int. Symp. on Advanced Topics in Electrical Engineering (ATEE) (Bucharest, Romania)* pp 1–6
[33] Zhang J L, Song C, Zhang J, Baker R and Zhang L 2013 Understanding the effects of backpressure on PEM fuel cell reactions and performance *J. Electroanal. Chem.* **688** 130–6
[34] Zhang J, Zhang H, Wu J and Zhang J 2013 *PEM Fuel Cell Testing and Diagnosis* 1st edn (UK: Elsevier) (https://doi.org/10.1016/C2009-0-63216-5)
[35] Zhang J, Tang Y, Song C, Cheng X, Zhang J and Wang H 2007 PEM fuel cells operated at 0% relative humidity in the temperature range of 23–120 °C *Electrochim. Acta* **52** 5095–101
[36] Rohendi D, Majlan E H, Mohamad A B, Daud W R W, Kadhum A A H and Shyuan L K 2015 Effects of temperature and backpressure on the performance degradation of MEA in PEMFC *Int. J. Hydrog. Energy* **40** 10960–8
[37] Cheng X, Zhang J, Tang Y, Song C, Shen J, Song D and Zhang J 2007 Hydrogen crossover in high-temperature PEM fuel cells *J. Power Sources* **167** 25–31
[38] Park Y H and Caton J A 2008 Monitoring an electrode flooding through the back pressure in a proton exchange membrane (PEM) fuel cell *Int. J. Green Energy* **5** 347–59
[39] Machado B S, Chakraborty N and Das P K 2017 Influences of flow direction, temperature and relative humidity on the performance of a representative anion exchange membrane fuel cell: a computational analysis *Int. J. Hydrog. Energy* **42** 6310–23
[40] Zhang J, Tang Y, Song C, Xia Z, Li H, Wang H and Zhang J 2008 PEM fuel cell relative humidity (RH) and its effect on performance at high temperatures *Electrochim. Acta* **53** 5315–21